Electrochemical cell design and performance evaluation of polyvinyl ferrocene/carbon nanotube electrodes for selective formate separation

Polat, Sevgi; Kortlever, Ruud; Eral, Hüseyin Burak

DOI
10.1016/j.seppur.2023.124554

Publication date
2023

Document Version
Final published version

Published in
Separation and Purification Technology

Separation and Purification Technology 324 (2023) 124554

Contents lists available at ScienceDirect

Separation and Purification Technology

journal homepage: www.elsevier.com/locate/seppur

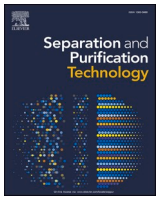

Electrochemical cell design and performance evaluation of polyvinyl ferrocene/carbon nanotube electrodes for selective formate separation

Sevgi Polat [a,b], Ruud Kortlever [c], Hüseyin Burak Eral [a,*]

[a] Complex Fluid Processing section, Process & Energy Department, Faculty of Mechanical, Maritime and Materials Engineering, Delft University of Technology, 2628 CB Delft, the Netherlands
[b] Chemical Engineering Department, Faculty of Engineering, Marmara University, 34854 İstanbul, Turkey
[c] Large-Scale Energy Storage section, Process & Energy Department, Faculty of Mechanical, Maritime and Materials Engineering, Delft University of Technology, 2628 CB Delft, the Netherlands

ARTICLE INFO

Keywords:
Electrochemical selective separation
Cell design
Electrosorption
Formate
Experimental design

ABSTRACT

Selective ion separation is a fundamental challenge with applications ranging from the manufacturing of pharmaceuticals & industrial salts to water desalination. In particular, the separation of formate, a primary product of electrochemical carbon dioxide reduction, has attracted attention not only to reduce carbon emissions and energy costs but to provide new routes to value-added chemicals. In the present study, selective formate separation from an aqueous solution is demonstrated using an electrochemical flow cell with symmetric redox-active polyvinyl ferrocene electrodes. An electrosorption system equipped with an electrosorption cell, inline conductivity, and pH sensors was constructed to provide real-time measurements of the formate adsorption performance in continuous flow mode while varying operating conditions such as the flow rate, cell voltage, and electrolyte concentration. These parameters were optimized using a Box–Behnken experimental design to improve the formate adsorption selectivity. The flow cell results showed a selectivity higher than 6.0 toward the removal of formate in an electrolyte containing a 30-fold excess of perchlorate under optimal operation conditions (i.e., 0.5 mL/min flow rate, 1.0 V, and 15 mM electrolyte concentration). The performance of the flow cell was also tested using a solution that contained different liquid CO_2 reduction products, and formate separation was achieved. The results suggest that the proper design of the electrochemical cell and efficient operation of the flow platform pave the way for scaling up the technology for selective formate separation.

1. Introduction

Climate change has been one of the major challenges of the past and will continue to be for the coming decades. Carbon dioxide (CO_2) is a major contributor to climate change. Over the past decade, global CO_2 emissions in the atmosphere have increased more than ever with values of 421 ppm in 2022, and this trend is expected to continue [1–3]. Roughly, 90% of human-made CO_2 emissions are the result of burning fossil fuels for industry making it by far the largest CO_2 contributor [4]. That's why new methods by which to produce carbon-based products must be found to produce renewable energy and reduce CO_2 emissions. An ideal situation would be a circular economy without any CO_2 being released into the atmosphere [5].

CO_2 can be electrochemically reduced to produce compounds with high added value and high market value per unit of energy. CO_2 electroreduction promises carbon–neutral chemical manufacturing when driven by renewable electricity. Depending on the choice of catalysts, carbon monoxide (CO), formate ($HCOO^-$), methane (CH_4), methanol (CH_3OH), ethylene (C_2H_4), ethanol (C_2H_5OH), acetate (CH_3COO^-), and *n*-propanol (*n*-C_3H_7OH) are typical products that are obtained [6–9]. Formate is an intriguing CO_2 reduction target product because it can be produced with high selectivities at relatively low overpotentials [10–13]. The electrochemical conversion of CO_2 into valuable products is a promising process; however, product separation remains a challenge since most of the products are typically produced within the millimolar to nanomolar concentrations range in the presence of a large excess of ions [14–16].

In addition to the electrochemical reduction of CO_2, the selective separation of organic anions within the chemical and pharmaceutical industries provides opportunities for significantly reducing capital

* Corresponding author.
E-mail address: h.b.eral@tudelft.nl (H.B. Eral).

https://doi.org/10.1016/j.seppur.2023.124554
Received 30 April 2023; Received in revised form 7 July 2023; Accepted 9 July 2023
Available online 13 July 2023

investment [17,18]. When compared to competing ions, such as electrolytes, buffers, byproducts, or catalysts, charged organic species are created in very low quantities within both industries, just as in electrochemical CO_2 reduction; therefore, selectively separating the carboxylates, sulfonates, and phosphonates found in several micropollutants using catalytic chemical processes remains a major challenge [19–22]. Specific organic ions can have significance for use in scientific and practical applications. One of these ions, formate, the smallest carboxylate, is an excellent example of this group. Although it is a key product in the CO_2 utilization process, separating it from homogeneous reaction mixtures remains difficult [23]. Both the development of CO_2 reduction technologies and the removal of impurities to produce clean water could benefit from the selective separation of formate ions.

Capacitive deionization (CDI) uses applied electric potentials to adsorb dissolved salts and micropollutants, which have an inherent electric charge, in the electric double layers created in porous electrodes; however, low adsorption capacity and co-ion expulsion effect have been limiting the practical implementation of CDI technology [24–28]. Apart from CDI, more recent electrochemical water treatment techniques, such as Faradaic CDI and electrochemically mediated selective ion adsorption, have gained a lot of attention primarily because of their higher capacity for salt adsorption and, more crucially, their selectivity for target ions [29–32]. Faradic CDI achieves ions removal through Faradic reactions involving the ions in the feed water being transferred into the Faradic electrodes by charge transfer [33–35]. Electrochemically mediated redox-active processes, based on heterogeneous redox-active organometallic compounds deposited on the surface of a carbon electrode, are gaining popularity as a viable liquid-phase separation technology. They are more advantageous than conventional systems because of their lower energy needs, non-destructive operation, lower footprint, modularity, scalability, and reversibility [36,37]. These features have obvious applications for societal and industrial problems, such as water treatment and chemical synthesis [38–41]. Because of these advantages, electrochemical separation techniques have recently come to the forefront to selectively separate formate ions from competing ions [42]; however, electrochemical separation remains limited to the scope of small lab-scale setups under static conditions. The current batch process should eventually be made continuous for increased throughput; however, the difference in scales indicates that several limitations that appear only for larger scales are not captured in small lab-scale. Su et al. [30] have reported a pseudocapacitive electrode based on metallocene ferrocene is remarkably selective toward nucleophilic organic functional groups such as carboxylates, sulfonates, and phosphonates (with separation factors > 140 against common electrolytes such as ClO_4^- and PF_6^-) under static conditions. He et al. [17] investigated the electrochemical mediated separation technique using symmetric redox-active electrodes (with an exposed surface of 2×2 cm) for selective removal of benzoate, as the target anion, in the presence of a 50-fold abundance of perchlorate electrolyte under flow conditions. The results showed a cycle selectivity of 3. Here, we intend to develop a continuous and larger scale separation setup for ion-specific selective technology specific for formate ions using recently developed lab-scale technology. In the present study, a large-scale electrosorption cell was designed and an electrosorption system was successfully constructed and operated in continuous flow mode to quantify the selectivity of formate separation in the presence of excess perchlorate electrolytes. The performance of the constructed continuous electrosorption system was significantly improved using an experimental design. In addition, the performance of the electrosorption system was tested using the solution remaining after CO_2 was reduced. The present study provides information on electrochemically mediated separations that address resource recovery from the reduction of CO_2.

2. Experimental section

2.1. Materials

Polyvinyl ferrocene (PVF, CAS number 34801–99-5) was purchased from Polysciences and was used without any further post-treatments. Multi-walled carbon nanotubes (CNTs, CAS number 308068–56-6), anhydrous chloroform (CAS number 67–66-3), potassium formate (CAS number 590–29-4), and lithium perchlorate (CAS number 7791–03-9) were obtained from Sigma Aldrich. Toray carbon paper (CP, TGP-H-60) was purchased from Alfa Aesar. Ultrapure water (Millipore MilliQ IQ 7000) was used to prepare the solutions.

2.2. Experimental methods

The experimental methods can be divided into four parts: i) fabrication and characterization of the PVF/CNT electrodes; ii) design of an electrochemical cell and construction of a continuous electrosorption system; iii) investigation of the total cycle charge efficiency and optimization of the conditions under which the highest charge efficiency for formate ions in electrosorption system; iv) separation of formate ions over perchlorate competing ions selectively.

2.2.1. Fabrication of PVF/CNT electrodes

The fabrication of the polyvinyl ferrocene/carbon nanotube (PVF/CNT) electrodes was previously described in our study on the ultrasound-intensified fabrication process for PVF functionalized electrodes in a CNT matrix [43]. This study highlighted the importance of electrode fabrication, and the optimal conditions were determined as PVF/CNT weight ratio of three, one hour ultrasonication time at 50 % ultrasonic amplitude, to provide the highest number of active surface sites and the highest adsorption efficiency for formate ion. Hence, we use a similar fabrication procedure here and refer the interested reader to our previous study [43]. In brief, the weighed quantity of PVF and CNT were added in a mass ratio of 3:1 ratio, dispersed in 10 mL anhydrous chloroform used as the solvent in a 20-mL glass vial, and sonicated (Cole-Parmer, Ultrasonic Processor) for one hour at 50% amplitude at a constant frequency to break down any agglomerates or aggregates into individual particles and to ensure homogeneity. During the sonication, the vial was sealed with parafilm to avoid any interactions with the surroundings and was kept inside an ice bath to minimize unnecessary extra heat generation that might trigger aggregation. After these steps, the PVF/CNT solution was ready for use, and the solution was drop cast onto one side of the electrode surface. Electrodes for electrochemical characterization were 1x2 cm, where the surface area exposed to the electrolyte was 1x1 cm and where functionalize by drop-casting 50 μL of PVF/CNT solution. The electrodes used in the flow cell were 8x8 cm, where the exposed surface area was 5x5 cm and where functionalized by drop-casting 250 μL of the PVF/CNT solution. After the drop casting, the electrodes were put in the oven to dry for 1 h at 30 °C to ensure all solvent is evaporated.

2.2.2. Electrochemical measurements and characterization

A three-electrode configuration consisting of a PVF/CNT working electrode, a platinum counter electrode, and an Ag/AgCl reference electrode was used for electrochemical tests. Cyclic voltammetry (CV) measurements were performed in a 15 mM $LiClO_4$ solution with a Biologic SP-200 potentiostat at a scan rate of 5 mV/s under an argon atmosphere at room temperature. Since the number of activated surface sites is directly related to the total charge passed during the oxidation of ferrocene, the charge can be calculated by integrating the area under the anodic peak of the CV. The area was determined with the Biologic EC-lab peak-analysis tool. Eq. (1) shows the relation between the charge and the measured current:

$$Q = \int_{t_1}^{t_2} Idt = \frac{1}{\nu}\int_{E_1}^{E_2} IdE \quad (1)$$

where Q is the charge (C), ν is the sweep rate (V/s) and E_1 and E_2 are the potentials where the anodic peak starts and ends (V).

In addition to the electrochemical analyses, the morphological characteristics of the fabricated PVF/CNT electrodes were investigated by scanning electron microscopy (SEM, Jeol JSM 6500F) with an accelerating voltage of 15 kV. High-performance liquid chromatography (HPLC, Agilent 1260 Infinity) was used to determine the concentration of formate ions before and after electrosorption.

2.2.3. Electrochemical cell design and construction of continuous electrosorption system

The electrosorption cell was designed using Rhinoceros 3D modelling software, and the configuration and a photograph of the electrochemical cell used are shown in Fig. 1a and 1b, respectively. The cell consists of two acrylic plates (80 by 80 by 4 mm), a pair of carbon paper electrodes, a rubber gasket, a polymer spacer, and titanium current collectors.

A laser cutter was used to manufacture the acrylic plates and gasket shown in Fig. 1a. The acrylic plate functioned analogous to a wall of an electrochemical cell, while the current collectors ensured contact with the electrode to realize a potential between the two electrodes. In addition, the gasket kept the electrodes in place and prevented any leakage, and the spacer prevented the two electrodes from making contact to prevent electrical short circuits. The holes within the end plates, gasket, and electrodes allowed for inlet and outlet flow. The carbon paper and polymer spacer were 0.205 and 0.05 mm thick, respectively. The coating thickness was approximately 50 μm and mass loading was about 40 mg. The dimensions of PVF/CNT electrodes manufactured for flow experiments were 5 by 5 cm. After constructing the cell, an electrosorption system for continuous separation was assembled. The continuous electrosorption system comprised of an electrochemical cell, peristaltic pump, influent and effluent containers, a power supply, and conductivity and pH probes. The conductivity and pH probes were used as inline sensors to evaluate the formate ion adsorption/desorption performance of the PVF/CNT electrodes under flow conditions. The schematic representation of the overall continuous electrosorption setup system is shown in Fig. 1c.

The feed solution was continuously pumped from the influent container into the electrochemical cell at a constant flow rate of 0.5 mL/min. The inlet was positioned at the bottom corner of the cell, and the outlet was positioned at the top corner as shown in Fig. 1b. Both conductivity and pH probes were placed near the outlet to continuously record changes in effluent conductivity and pH, respectively. While the feed solution was pumped through the cell, positive and negative potentials were applied for a set time. The power was provided using a source meter (Keithley, SMU 2450). The cell was charged by applying 1.0 V for 5 min followed by a discharging step at −1.0 V for 5 min. This cycle of applying and removing voltage was repeated several times. The software of the source meter recorded any change in current value. The samples taken from the effluent were measured using high-performance liquid chromatography (HPLC) to determine the amount of formate adsorbed. Each experiment was cycled at least five times and repeated at least three times. The total cycle charge efficiency of the process, defined as the amount of formate removed per charge passed, was calculated as:

$$\Lambda = \frac{q_{formate}}{q_{charge}} = \frac{Q\int(C_{in} - C)dt}{\int Idt/F} \quad (2)$$

where C_{in} and C are the initial and final anions/cations concentrations, Q is the volumetric flow rate, F is Faraday constant.

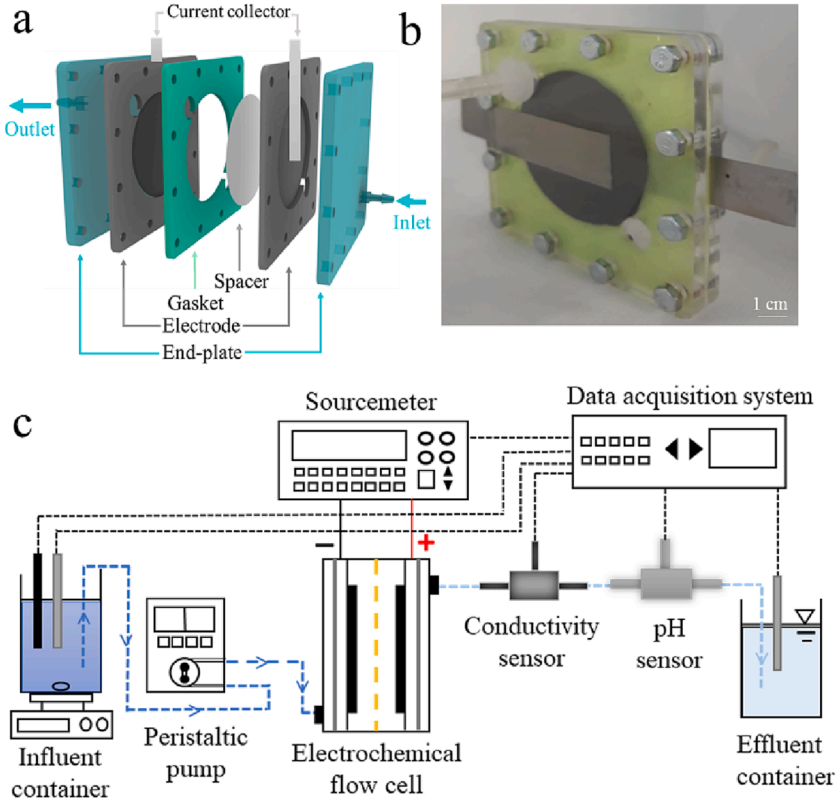

Fig. 1. (a) Exploded view three-dimensional (3D) drawing, and (b) photograph of the electrochemical cell. The cell stack consists of two-end plates, two electrodes, a spacer, a gasket, and current collectors. (c) Schematic representation of our electrosorption system with influent and effluent containers, the peristaltic pump, the electrochemical cell, a power source, and inline sensors including an electroconductivity sensor and a pH sensor.

2.2.4. Experimental design and statistical analyses

To optimize the performance of selective formate adsorption in the flow cell, it was necessary to understand how the operating conditions affected the efficiency of the cycle charge. Design models reduce the number of trials, save time and money, and decrease the amount of materials needed. In the present study, the Box–Behnken design (BBD) combined with the response surface method (RSM) was applied to investigate the statistical relationships between independent variables (i.e., flow rate [A], cell voltage [B], and electrolyte concentration [C]) and total cycle charge efficiency as a response. $LiClO_4$ solution was used as the electrolyte. These levels have been considered as variables that may potentially affect the response functions and were selected based on preliminary experiments. The experimental runs were performed based on a three-factor, three-level BBD, which entailed a set of midpoints points and a replicated central point in the multidimensional cube using 15 experiments, as computed by Design Expert (Eq. (3).

$$N = 2k(k-1) + C_0 = 2 \times 3(3-1) + 3 = 15 \quad (3)$$

where N is the number of the experiments, k is the number of independent variables and C_0 is the replicate number of central point. Each experiment in the study was conducted at least three times. The levels and ranges of the variables used in the present study are listed in Table 1.

Following the experiments, we used a second-order polynomial regression model equation to determine the mathematical relationship between the response function and the process variable. The general form of this equation is as follows:

$$Y = \beta_0 + \sum_{i=1}^{k} \beta_i X_i + \sum_{i=1}^{k} \beta_{ii} X_i^2 + \sum_{i_{i=1}}^{k} \sum_{j>1}^{k} \beta_{ij} X_i X_j \quad (4)$$

where Y shows the predicted response, β_0 is the constant term, β_i is the linear coefficient, β_{ii} is the quadratic coefficient, and β_{ij} is the interaction coefficient.

The experimental designs were analyzed, and the response surface plots were generated by Design Expert software (https://www.statease.com/software/design-expert/). The statistical fitness, accuracy and validity of the developed Box-Behnken model were checked by the analysis of variance (ANOVA). The coefficient of determination, R^2, and F-test were used to assess the model validation while comparing the calculated values with the predicted values.

3. Results and discussion

3.1. Electrode preparation

The functionality of a synthesized electrode is determined by its electrochemical characterization; therefore, the electrochemical characterization of the constructed PVF/CNT electrode was conducted using cyclic voltammetry (CV). CV measurements were conducted using a three-electrode setup in a 15 mM $LiClO_4$ aqueous electrolyte (Fig. 2a). Fig. 2b shows the CV curves of the electrodes functionalized with PVF, CNT, and PVF/CNT.

The basic shapes of the CV curves for the electrodes with PVF and PVF/CNT had similar shapes at a first glance; however, two main differences were observed. First, both the anodic and cathodic peak potentials showed a shift depending on the incorporation of CNT into the PVF film, which changed the peak potentials for ferrocene oxidation.

Table 1
Range and levels of variables in Box–Behnken experimental design.

Design variable	Symbol	Range and levels		
		−1	0	1
Flow Rate (mL/min)	A	0.5	5	9.5
Cell Voltage (V)	B	0.75	1	1.25
Electrolyte Concentration (mM)	C	5	10	15

Additionally, the peak current for both the oxidation and reduction was significantly higher with the PVF/CNT electrodes than with the electrodes containing solely PVF or CNT. The voltammogram of the PVF/CNT electrode showed an anodic peak current of 2.1 mA at 0.48 V and a cathodic peak current of −1.8 mA at 0.22 V, whereas the voltammogram of the PVF electrode showed an anodic peak current of 0.28 mA at 0.40 V and a cathodic peak current of −0.16 mA at 0.30 V. This increase in the current response was attributed to the incorporation of highly conductive carbon nanotubes into the PVF film, which reduces the charge transfer resistance in the polymer matrix and, as a result, enables more effective ferrocene oxidation and reduction. Second, the areas for both the anodic and the cathodic peaks were higher with the PVF/CNT electrode, indicating that the performance of the electrode is highly dependent on the deposition. Oxidized ferrocene units on the electrode surface selectively adsorbed formate from the solution [43]. The number of active oxidized ferrocene surface sites is directly related to the area under the anodic peak curve, indicating the charge, which was proportional to the amount of PVF deposited. The PVF/CNT co-deposited electrode had the highest charge at 62.8 ± 3.1 mC. Fig. 2c shows the electrochemical performance of the PVF/CNT electrode. The results show that the voltammograms of five cycles are very similar, indicating that the fabricated electrodes were reversible and stable in the used perchlorate electrolyte.

In addition to electrochemical measurements, the morphological characterization of the prepared electrodes at different PVF/CNT loadings was investigated. The scanning electron microscope (SEM) images are provided in Fig. 2d. The surface of the untreated carbon paper electrode is composed of smooth carbon fibers with a diameter of ~10 μm, which is similar to the previous studies. [44,45]. When the electrodeposited CP/CNT electrode was examined, it was determined to be similar to the untreated CP electrode and had nearly the same morphology. Thus, the use of CNT alone had nearly no effect on the coating of the carbon surface; however, the electrodeposited CP/PVF electrode was different than the untreated CP electrode. A polymer layer consisting of hollow structures covering the surface in an inhomogeneous manner is observed. This is expected because the nature of a polymer on an electrode surface becomes oxidized and solvophobic. When the SEM of the electrodeposited PVF/CNT electrodes was examined, the surface of the electrodes was smooth, uniform, homogeneously dispersed, and had pores of uniform size and micropores that were interconnected with a 3D framework and surrounded by a conformal polymer coating. A stable film was created and dispersed on the substrate by the π–π interaction between ferrocene moieties and CNTs. The electrons then quickly migrated from the carbon fiber substrate to the redox-active center of the polymer [20,46,47]. Our previous study [43] has shown that proper coating of the electrode surfaces significantly affects the electrochemical performance of the electrode and thus formate adsorption efficiency; therefore, these electrodes produced under optimized conditions were used in the flow system experiment.

3.2. Flow system results

After fabrication and characterization of the PVF/CNT electrodes at the small scale (2 by 1 cm), the performance of our electrochemical cell (8 by 8 cm) was tested under realistic conditions at constant voltage and continuous flow of a supporting electrolyte in the absence of formate ions. Normally, ferrocene is an electroneutral compound but ferrocene Fe(II) is oxidized to ferrocenium Fe(III) and acts as a mild electrophilic center after applying a potential across the cell. This event enables the formed ferrocenium center to selectively adsorb nucleophilic organic functional groups such as carboxylates, sulfonates, and phosphonates. A benefit of PVF is that its highly soluble in organic solvents and can disperse large amounts of CNTs in organic solvents with great dispersion quality. Stable dispersions between two components can be established due to the unique ability of the metallocene/carbon system using π-π stacking interactions. This results in a hybrid pseudo-capacitive device

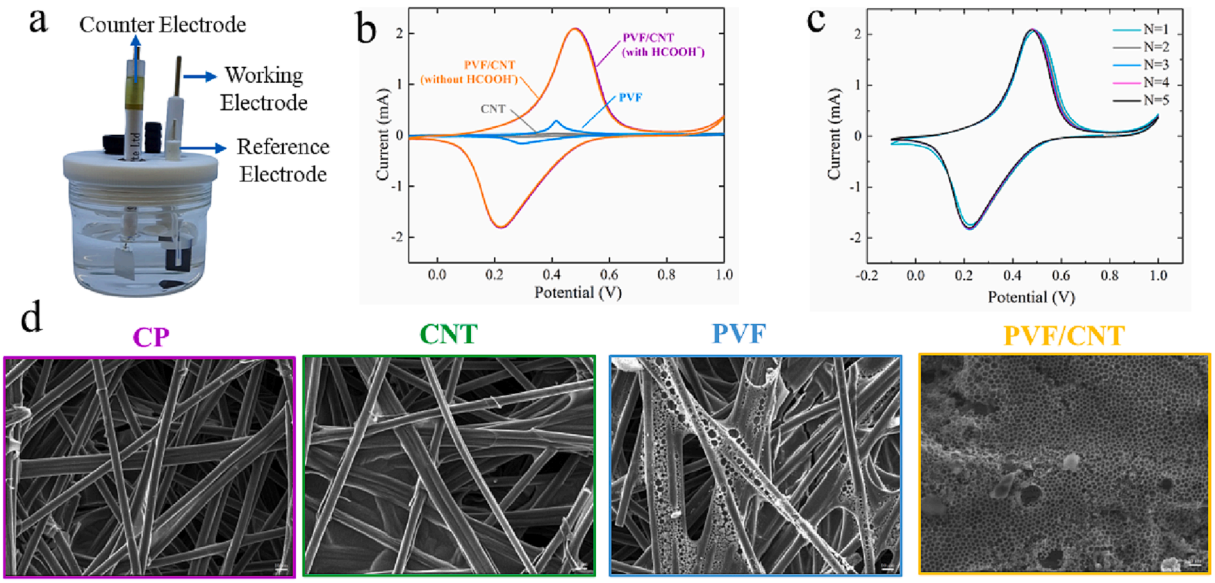

Fig. 2. (a) The image of a three-electrode electrochemical cell. (b) Cyclic voltammograms of individual CNT (grey line), PVF (blue line), PVF/CNT (orange line- without formate), and PVF/CNT (purple line- with 0.5 mM formate) electrodes under Ar in 15 mM $LiClO_4$ electrolyte at the scan rate of 5 mV/s. (c) Electrochemical stability of the fabricated PVF/CNT electrode. (d) Scanning electron microscopy (SEM) images of untreated carbon paper (CP) electrode, carbon paper electrode treated by electrochemical oxidation in the CNT/chloroform dispersion, PVF/chloroform dispersion, and PVF/CNT chloroform dispersion. (For interpretation of the references to colour in this figure legend, the reader is referred to the web version of this article.)

with high power and high energy density interactions. Some of these specific interactions are energetically more favorable for some ions than others, resulting in increased selectivity towards specific ions. The selectivity towards nucleophilic organic groups such as formate is larger due to the fact that redox-enhanced hydrogen bonding of ferrocene cyclopentadienyl ring [20,47]. A schematic illustration of the flow cell with redox-active PVF/CNT electrodes is shown in Fig. 3. The basic operation principle of this flow cell can be separated into three steps as follows: (1) uncharged, (2) adsorption/charging, and (3) desorption/discharging. First, the cell was fed with 10 mM $LiClO_4$ electrolyte at a constant flow rate of 0.5 mL/min. During the uncharged step, redox-active moieties were present on both the anode and cathode, after which the electrodes were connected to the power source and charged at 1.0 V for 5 min for adsorption and discharged at −1.0 V for 5 min for desorption. This cycle was repeated throughout the experiment for five consecutive cycles to ensure a dynamic steady state. During the electrochemical measurement, the voltage between the electrodes was stepped to 1.0 V for 5 min, and the redox moieties on the anode were

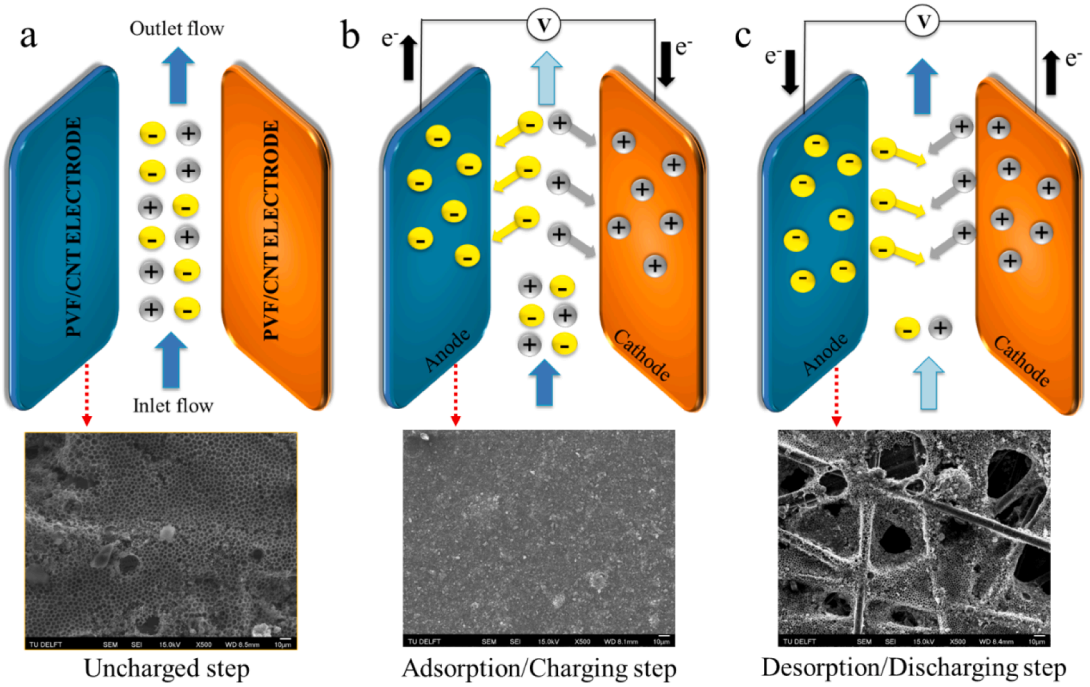

Fig. 3. Schematic illustration of the flow cell with redox-active PVF/CNT electrodes for (a) uncharged step, (b) adsorption step, and (c) desorption step during the electrosorption process. Scanning electron microscopy (SEM) images of the PVF/CNT electrodes obtained treated by electrochemical oxidation for (a) uncharged step, (b) adsorption step, and (c) desorption step.

oxidized to ferrocenium with a net positive charge. The applied charge caused anions to be adsorbed from the influent through hydrogen bonding and electrostatic attraction to control the adsorption strength [17]. After this charging phase, the applied potential was removed and the electrodes regenerated by setting the voltage difference to −1.0 V, applying a reverse potential. The applied voltage step and current response are illustrated in Fig. 4a.

As clearly seen in Fig. 4a, the measured current spikes initially but quickly dropped off while the charging phase proceeded. Immediately after the change in applied voltage, the driving force for electrosorption was at maximum and many anions from the electrolyte were adsorbed, resulting in a peak current. Over time the current decayed rapidly as the surface became more and more saturated with adsorbed species. After 5 min of charging, the applied electrostatic potential was set to −1.0 V and an inverted current response was observed. The ionic charge that built up in the electrode was allowed to move out of the electrode, which then released the adsorbed ions back into the solution. The effluent's conductivity and pH were continuously recorded during the experiments to determine the cell's performance. The profiles of the effluent concentration and pH of perchlorate ions are shown in Fig. 4b. The curves showed typical adsorption/desorption behavior. Applying the voltage across the electrodes in the cell resulted in a net electrolyte concentration drop (analogous to the sharp increase in measured current), which occurred because of ion adsorption on the electrode surface. The

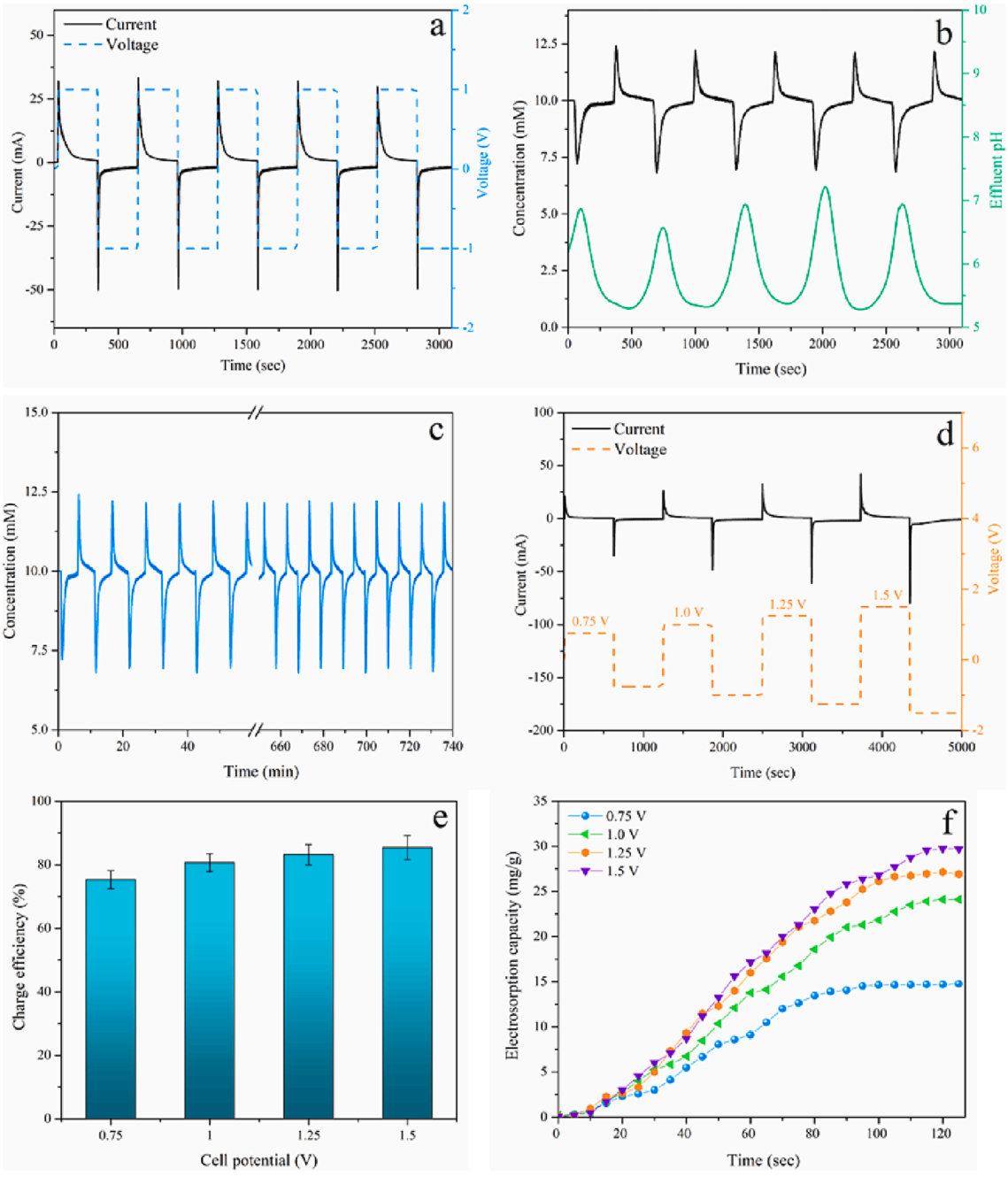

Fig. 4. Cycling performance of symmetric redox-active electrode pair under charging at 1.0 V and discharging at −1.0 V cell voltage in 10 mM $LiClO_4$ electrolyte solution. (a) Current and voltage profiles and (b) the effluent concentration and pH of perchlorate ions. (c) Cycling performance of symmetric redox-active electrode pair under different charging and discharging cell voltage in 10 mM $LiClO_4$ electrolyte solution. (d) Current and voltage profiles, (e) the charge efficiencies, and (f) corresponding electrosorption capacities with respect to the applied potential.

charged ions were drawn to the oppositely polarized electrodes and stored in the pore structure. The deionized solution passed through the cell and once it exited the cell, its conductivity was measured. The electrodes became saturated over time, which gradually increased the concentration of the solution until nearly reaching its initial value. In addition, a sharp increase in concentration was observed during the discharge step because the adsorbed ions from the earlier step were desorbed to the electrolyte; therefore, a high concentration was recorded initially and later gradually decreased to approach the initial concentration (Fig. 4b). That is, after 5 min of charging, the electrodes were regenerated and a sharp increase in concentration was observed. All adsorbed ions were released from the electrodes and a concentrated solution was formed. In time, the concentration returned to its initial value and the electrodes were fully regenerated. In addition, it was observed that the five adsorption/desorption cycles behaved similarly and showed the that a dynamic steady state was reached. The variation in pH was also recorded during the electrosorption process, with a change between 5.5 and 7.0. An increase in pH was observed during the adsorption stage; whereas, the pH decreased during the desorption stage.

Fig. 4c shows the prolonged cycling performance of the PVF/CNT electrodes and the profile kept stable after 12 h of cycling, demonstrating the high reversibility of the electrodes. In addition to the experiments with an adsorption potential at 1 V, experiments were conducted at varying potentials ranging from 0.75 to 1.50 V in 10 mM $LiClO_4$ electrolyte at a constant flow rate of 0.5 mL/min. Fig. 4d and 4e compare the voltage/current profiles and the charge efficiencies with respect to the applied potential. As clearly seen in Fig. 4d, a larger applied voltage leads to an increased current and provides larger charge efficiency of the flow-cell. At 1.5 V, the charge efficiency reached the highest value of 85.4%. Fig. 4f shows the higher voltages were favorable for electrosorption because the resulting electric field was stronger. In addition, the increased voltage enabled a more rapid rate of electrosorption, with the highest capacity of 29.68 mg/g occurring at 1.5 V—a significant improvement from the result of the lower voltage.

3.3. Experimental design results

A BBD experimental design was used to investigate the effects of three independent variables—flow rate (A), cell voltage (B), and electrolyte concentration (C)—on the response function to determine the conditions that maximized the process efficiency and, thus, formate adsorption performance. Table 2 shows the process variables, their actual and coded values, and the measured responses. Based on these results, a second-order polynomial equation representing an empirical relationship between the response and the independent variables in terms of coded factors for total cycle charge efficiency (CE) was developed as follows:

$$Y_{CE} = 72.07 - 8.75A + 3.46B + 2.01C - 0.075AB - 1.13AC - 0.65BC - 1.73A^2 + 0.94B^2 + 1.69C^2 \quad (5)$$

Signs (+/-) and magnitudes of the coefficients in the above second-order polynomial equation show the effect of the independent variables on the response (i.e., efficiency of the process). Negative coefficients show an unfavorable effect and the inverse relationship between the response and the variable, while positive coefficients indicate a favorable effect and direct relationship on the total cycle

Table 2
Box-Behnken experimental design matrix and results.

RunOrder	Actual level of variables			Coded level of variables			Response
	Flow Rate	Cell Voltage	Electrolyte Concentration	A	B	C	Total Cycle Charge Efficiency (%)
1	5	0.75	5	0	−1	−1	69.4
2	5	1.25	5	0	+1	−1	76.8
3	5	0.75	15	0	−1	+1	73.9
4	5	1.25	15	0	+1	+1	78.7
5	0.5	0.75	10	−1	−1	0	75.3
6	0.5	1.25	10	−1	+1	0	83.2
7	9.5	0.75	10	+1	−1	0	59.5
8	9.5	1.25	10	+1	+1	0	67.1
9	0.5	1.0	5	−1	0	−1	78.0
10	0.5	1.0	15	−1	0	+1	85.1
11	9.5	1.0	5	+1	0	−1	61.2
12	9.5	1.0	15	+1	0	+1	63.8
13	5	1.0	10	0	0	0	72.1
14	5	1.0	10	0	0	0	71.7
15	5	1.0	10	0	0	0	72.4

Table 3
ANOVA results of the response surface quadratic model for total cycle charge efficiency (%).

Source	Sum of Squares	df	Mean Square	F-Value	p-value Prob > F
Model	774.38	9	86.04	55.34	0.0002
A-Flow Rate	612.50	1	612.50	393.93	< 0.0001
B- Cell Voltage	95.91	1	95.91	61.69	0.0005
C-Electrolyte Concentration	32.40	1	32.40	20.84	0.0060
AB	0.022	1	0.022	0.014	0.9089
AC	5.06	1	5.06	3.26	0.1310
BC	1.69	1	1.69	1.09	0.3449
A^2	11.09	1	11.09	7.13	0.0443
B^2	3.27	1	3.27	2.11	0.2065
C^2	10.57	1	10.57	6.80	0.0478
Residual	7.77	5	1.55	–	–
Lack of Fit	7.53	3	2.51	20.34	0.0472
R^2	0.9901				

Adj $R^2 = 0.9722$, Pred $R^2 = 0.8453$, Adequate Precision = 24.334, Standard Deviation = 1.25.

charge efficiency. Looking at Eq. (5), it is observed that flow rate had the highest effect on the total cycle charge efficiency. As the flow rate decreased, a significant increase in total cycle charge efficiency was observed due to the negative coefficient of the flow rate. Because the coefficient of electrolyte concentration was very small compared to other coefficients, it can be proposed that electrolyte concentration had the least effect. Because the coefficients of the cell voltage and electrolyte concentration were positive, the cycle efficiency increased with an increase in these parameters.

Analysis of variance was used to determine the significance of this quadratic model. The F-test was also applied to estimate significance. The high F-value demonstrated that the developed regression equation could adequately account for the majority of the output variation. To determine whether F was large enough to show statistical significance, the associated p-value was also used as a guide. Table 3 summarizes the results from ANOVA that was used to assess the significant effects and interactions.

In the present study, the F-value, which shows that the model was statistically significant, was calculated as 55.34 and the p-value was <0.0002, indicating that there was only a 0.02% chance that noise

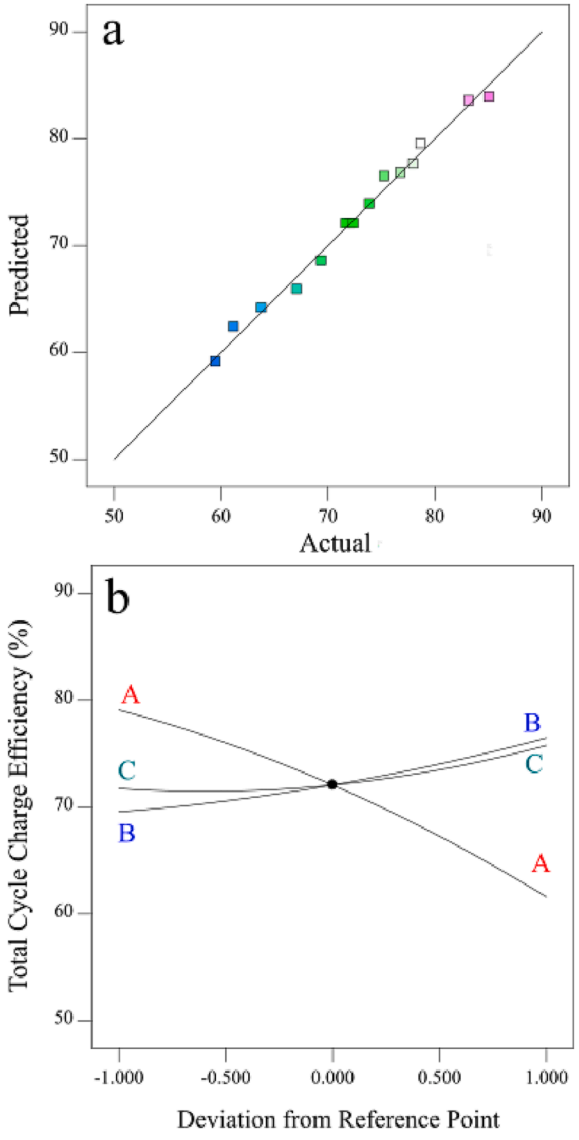

Fig. 5. (a) The plot of predicted versus actual values and (b) the perturbation plot of each factor (A: Flow rate, B: Cell voltage, and C: Electrolyte concentration) for total cycle charge efficiency (%).

influenced the F-value. From the p-values of each model terms, it can be suggested that the independent parameters A, B, and C; and the quadratic terms A^2 and C^2 were significant and indicated the pattern of the interactions among the variables. Considering the F values for the quadratic model terms, the effect order of the variables on the total cycle charge efficiency is A > B > C. In other words, the flow rate was determined as the most influential independent variable with the highest F-value. The model determination coefficient, R^2, showing the quality of the fit of the model value, was obtained as 0.9901. Pred R^2 and Adj R^2 values were calculated as 0.8453 and 0.9722, which are statistically compatible. Adeq Precision was used for measuring the signal to noise ratio, which is considered desirable if it is >4. In this study, it was determined as 24.334. Therefore, the design space is suitable for the three-dimensional (3D) graphical representation of the results and this model is significant for this electrochemical separation process. Fig. 5a and 5b shows the relationship between the actual and predicted values of response and the simultaneous effect of three factors on total cycle charge efficiency, respectively. It is seen in Fig. 5 that the developed model was adequate as the predicted values obtained were quite close to the experimental values.

Using RSM, the effects of the independent variables on charge efficiency were plotted in 3D response surface plots and 2D contour plots. As a function of two factors, 3D response surfaces and their corresponding contour plots provided deeper insight into both the main and the interaction effects of these two factors while keeping all other parameters at constant levels. The effects of flow rate and cell voltage (a), flow rate and electrolyte concentration (b), and cell voltage and electrolyte concentration (c) on the total cycle charge efficiency are given in Fig. 6.

The main aim of the response surface is to monitor variables efficiently for the optimum values to maximize the response. The best response range can be calculated by analyzing the plots. Considering the 3D and 2D plots together, a desirable high response value was achieved with a lower flow rate and higher cell voltage. As the applied cell voltage increased, a comparable increase in the total cycle charge efficiency was observed. It was also observed that as the flow rate of the feed solution decreased from 9.5 to 0.5 mL/min, the cycle efficiency increased from 67.1 to 83.2% at constant electrolyte concentration. Compared to cell voltage and electrolyte concentration, flow rate was the most significant parameter, affecting total cycle charge efficiency response. In this study, the optimum conditions were found to be 0.5 mL/min flow rate, 1.0 V, and 15 mM electrolyte concentration.

3.4. *Selective formate recovery in flow-cell system*

Thanks to the prepared PVF/CNT redox-active electrodes, anions can adsorb at the anode and cations can adsorb at the cathode. The electrodes demonstrated ion adsorption behavior during the charge step and released the ions to the solution during the discharge step when paired and tested for applications of selective separation of ions. The process exhibited strong electrosorption behavior when the cell operation alternated between adsorption and desorption modes. In addition, our results showed that the total cycle charge efficiency of the process was >85% under optimized operating conditions. After testing and optimizing the performance of the flow-cell system, the selective separation of formate ions was conducted under flow conditions. The results are given in Fig. 7.

As stated in the literature [17], hydrogen bonding causes a reaction between the conduction polymer in the charged state (i.e., ferrocenium) and anions. This bonding is caused by the substituent groups from which electrons are withdrawn and is much stronger than the electrostatic interaction with anions. We quantified formate removal selectivity with respect to the background electrolyte. A feed solution containing 0.5 mM formate and 15 mM $LiClO_4$ (a 30x mixing ratio) was used to evaluate formate selectivity with respect to the background anion. In other words, while formate (0.5 mM) was the target anion, perchlorate (15

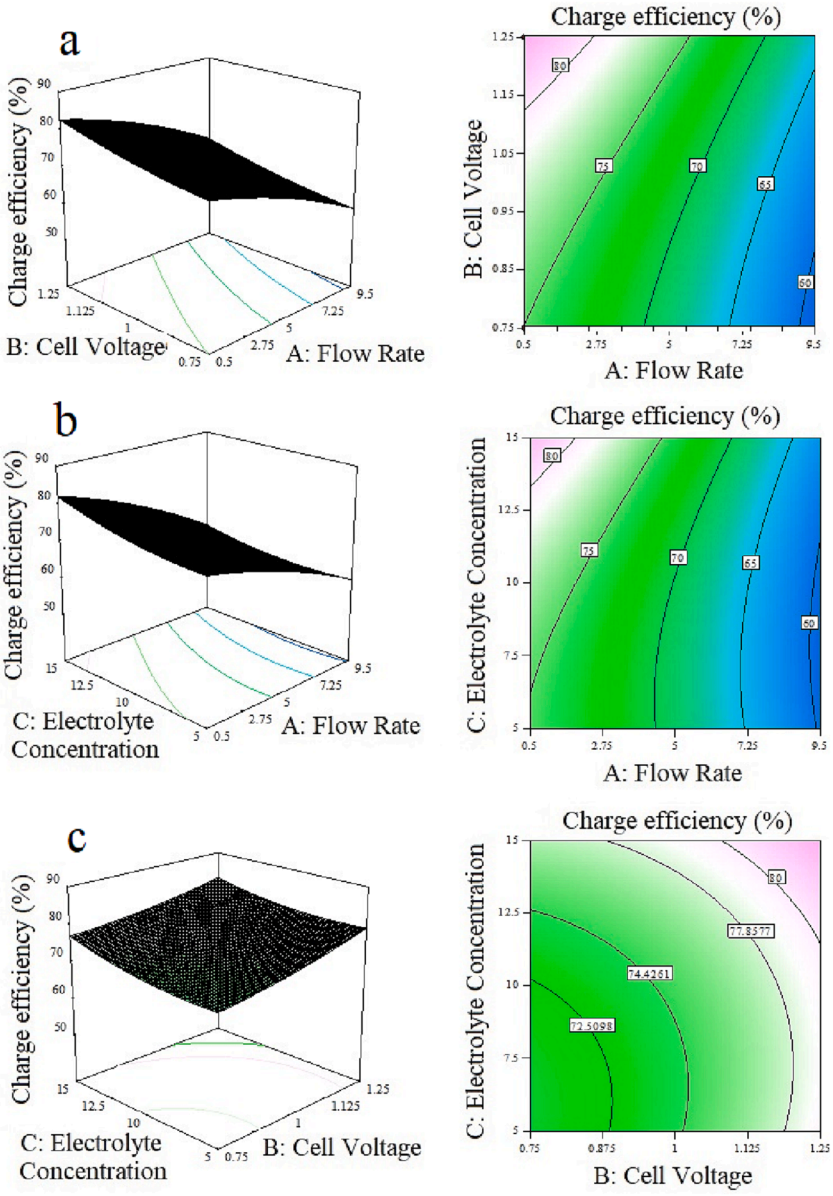

Fig. 6. Three-dimensional (3D) response surface plots and two-D (2D) contour plots indicating the effects of (a) flow rate and cell voltage, (b) flow rate and electrolyte concentration, and (c) cell voltage and electrolyte concentration on the total cycle charge efficiency (%).

mM) was the competing anion. To determine the formate concentration, aliquots of 100 μL were drawn from the effluent after every cycle for HPLC measurements. We calculated the selectivity of formate ions against the perchlorate ions as follows:

$$S_{formate} = \frac{(\Delta C/C_0)_{formate}}{(\Delta C/C_0)_{perchlorate}} \quad (6)$$

where C_0 is the initial concentration (0.5 mM here) and ΔC is the change in concentration after a given time. Under flow conditions at 30-fold supporting anions, cycle selectivity was 6.2 ± 1.1 for first cycle. The selectivity of each cycle was very similar to each other. The significant excess of the anion provided for rapid perchlorate ion adsorption and ferrocenium stabilization on the electrode surface compared to that of formate; however, over time, adsorption of formate on the electrode was observed. With its higher binding strength than perchlorate, formate displaced perchlorate anions, which eventually resulted in a ratio of adsorbed formate to perchlorate of 6.2 times higher than that in the feed stream.

The SEM images of the PVF/CNT electrodes obtained at uncharged, charging, and discharging steps within the flow-cell system are provided in Fig. 3b. With this fabricated electrode under optimum conditions during the uncharged step, easy access could be provided for ions where the active material interfaces with the electrolyte. The diffusion path could be reduced and the electrochemical performance of the electrode could be enhanced because of the porous structure. When the SEM images of the electrode after adsorption of formate ions are examined, the surface morphology of the optimized electrode during the uncharged step was observed to have completely changed and nearly all voids on the surface were filled with the formate ion; however, as a result of the desorption process, larger, irregular holes were formed on the electrode surface.

3.5. Application results

In the present study, after ensuring that the electrochemical cell worked well under flow conditions, the selective separation of formate ions was investigated using the solution obtained in the CO_2 electrolysis processes to simulate more realistic conditions. The CO_2 reduction

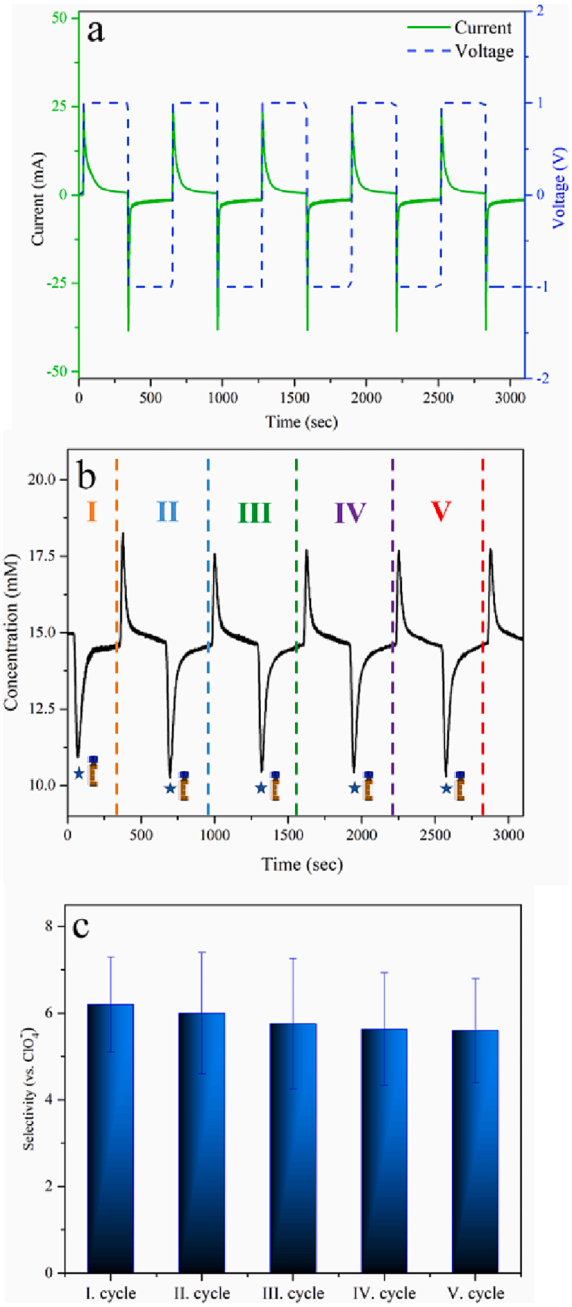

Fig. 7. Selective removal of formate from aqueous solution in the presence of perchlorate ions using PVF/CNT redox-active electrodes. (a) Current and voltage profiles and (b) the effluent concentration under charging at 1.0 V and discharging at −1.0 V cell voltage in 0.5 mM formate and 15 mM $LiClO_4$ electrolyte. (c) Calculated selectivity of formate ions with respect to perchlorate ions (in 30-fold abundance) for each cycle.

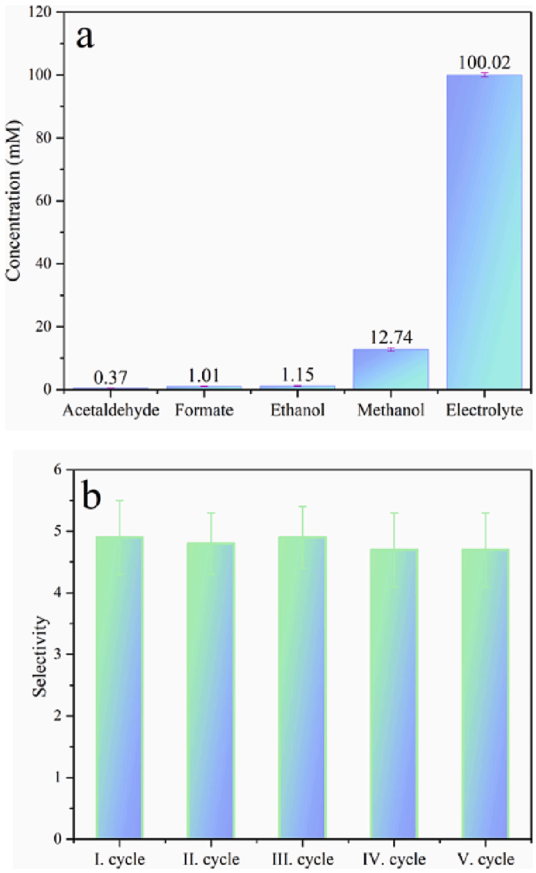

Fig. 8. Selective removal of formate from CO_2 liquid product using PVF/CNT redox-active electrodes. (a) The initial content of the liquid sample. (b) Calculated selectivity of formate ions with respect to bicarbonate electrolyte in 100-fold abundance for each cycle.

reaction was conducted at different potentials in CO_2 saturated 0.1 M $KHCO_3$ solution using an H-type cell. An anion exchange membrane was used as a separator to avoid oxidation of CO_2 reduction products. After 1 h of electrolysis, a liquid sample was collected. This liquid solution contained the products formed as a result of the electrochemical reduction of CO_2 in 0.1 M saturated $KHCO_3$ electrolyte at different potentials. First, the initial content of the solution was determined using HPLC and the results are given in Fig. 8. When the results were examined, the concentration of the formate ion was 1% of the electrolyte solution used. In addition, methanol, ethanol, and small amount of acetaldehyde were detected in the solution, which was expected. The same voltage values were applied to the cell for the adsorption (1.0 V for 5 min) and desorption (-1.0 V for 5 min) steps under a single pass flow of 0.5 mL/min. The results showed selectivity of > 4.7 toward formate compared to a liquid product, including the bicarbonate electrolyte in 100-fold abundance. This technology as demonstrated would require that the electrodes remain stable over several adsorption/desorption cycles and the use of high active material loading and large electrode areas to achieve capacity high enough for industrial applications.

4. Conclusion

A scalable continuous electrosorption system based on an electrochemical cell with symmetric PVF/CNT redox electrodes was successfully designed to selectively remove formate ions from aqueous solution. First, the fabricated PVF/CNT electrodes were characterized electrochemically, and the CV results indicated that the prepared electrodes at stable upon cycling. SEM images revealed that the fabricated electrodes had a porous surface with a high coating yield. The performance of the constructed flow platform was improved by optimizing the conditions using an experimental design. The BBD results showed that two variables tested (i.e., cell voltage and electrolyte concentration) were positively related to the efficiency of the total cycle charge. The optimal operation conditions were 0.5 mL/min, 1.0 V, and 15 mM electrolyte concentration, with a selectivity of 6.2 ± 1.1 toward formate compared to a 30-fold abundance of perchlorate electrolyte. The present study may provide new insights into the design and operation of an electrochemical system for formate separation on a larger scale.

CRediT authorship contribution statement

Sevgi Polat: Conceptualization, Methodology, Investigation, Validation, Visualization, Writing – original draft, Writing – review & editing. **Ruud Kortlever:** Conceptualization, Supervision, Writing – review & editing. **Hüseyin Burak Eral:** Conceptualization, Project administration, Supervision, Writing – review & editing.

Declaration of Competing Interest

The authors declare that they have no known competing financial interests or personal relationships that could have appeared to influence the work reported in this paper.

Data availability

Data will be made available on request.

Acknowledgements

S. Polat would like to acknowledge financial support from the Scientific and Technological Research Council of Turkey (TUBITAK 2219) [Grant No: 1059B192000847]. The authors thank Dr. Ahmed Mohsen Ismail for providing the solution obtained in the CO_2 electrolysis processes.

References

[1] M.N. Hossain, R.M. Choueiri, S. Abner, L.D. Chen, A. Chen, Electrochemical Reduction of Carbon Dioxide at TiO2/Au Nanocomposites, ACS Appl. Mater. Interfaces. 14 (2022) 51889–51899, https://doi.org/10.1021/acsami.2c14368.
[2] K. Nguyen, I. Iliuta, F. Bougie, L.C. Pasquier, M.C. Iliuta, Techno-economic assessment of enzymatic CO2 capture in hollow fiber membrane contactors with immobilized carbonic anhydrase, Sep. Purif. Technol. 307 (2023), https://doi.org/10.1016/j.seppur.2022.122702.
[3] K.P. Dhaneesh, P. Ranganathan, A comprehensive review on the hydrodynamics, mass transfer and chemical absorption of CO2 and modelling aspects of rotating packed bed, Sep. Purif. Technol. 295 (2022), 121248, https://doi.org/10.1016/j.seppur.2022.121248.
[4] S. Roy, A. Cherevotan, S.C. Peter, Thermochemical CO2 Hydrogenation to Single Carbon Products: Scientific and Technological Challenges, ACS Energy Lett. 3 (2018) 1938–1966, https://doi.org/10.1021/acsenergylett.8b00740.
[5] A. Taheri Najafabadi, CO2 chemical conversion to useful products: An engineering insight to the latest advances toward sustainability, Int. J. Energy Res. 37 (2013) 485–499, https://doi.org/10.1002/er.3021.
[6] P. Kang, S. Zhang, T.J. Meyer, M. Brookhart, Rapid selective electrocatalytic reduction of carbon dioxide to formate by an iridium pincer catalyst immobilized on carbon nanotube electrodes, Angew. Chemie - Int. Ed. 53 (2014) 8709–8713, https://doi.org/10.1002/anie.201310722.
[7] Y. Luo, K. Zhang, Y. Li, Y. Wang, Valorizing carbon dioxide via electrochemical reduction on gas-diffusion electrodes, InfoMat. 3 (2021) 1313–1332, https://doi.org/10.1002/inf2.12253.
[8] R. Kortlever, J. Shen, K.J.P. Schouten, F. Calle-Vallejo, M.T.M. Koper, Catalysts and Reaction Pathways for the Electrochemical Reduction of Carbon Dioxide, J. Phys. Chem. Lett. 6 (2015) 4073–4082, https://doi.org/10.1021/acs.jpclett.5b01559.
[9] S. Fu, M. Li, S. Asperti, W. de Jong, R. Kortlever, Unravelling the effect of activators used in the synthesis of biomass-derived carbon electrocatalysts on the electrocatalytic performance for CO2 reduction, ChemSusChem. (2023), https://doi.org/10.1002/cssc.202202188.
[10] C. Chen, J.F. Khosrowabadi Kotyk, S.W. Sheehan, Progress toward Commercial Application of Electrochemical Carbon Dioxide Reduction, Chem. 4 (2018) 2571–2586, https://doi.org/10.1016/j.chempr.2018.08.019.
[11] S. Van Daele, L. Hintjens, J. Van Den Hoek, S. Neukermans, N. Daems, J. Hereijgers, T. Breugelmans, Influence of the target product on the electrochemical reduction of diluted CO2 in a continuous flow cell, J. CO2 Util. 65 (2022), https://doi.org/10.1016/j.jcou.2022.102210.
[12] D. Ewis, M. Arsalan, M. Khaled, D. Pant, M.M. Ba-Abbad, A. Amhamed, M.H. El-Naas, Electrochemical reduction of CO2 into formate/formic acid: A review of cell design and operation, Sep. Purif. Technol. 316 (2023), 123811, https://doi.org/10.1016/j.seppur.2023.123811.
[13] X. Zhang, X. Jiao, Y. Mao, X. Zhu, H. Kang, Z. Song, X. Yan, X. Yan, C. Han, L. Cui, K. Zhang, J. Qiao, A BiPb bimetallic electrode for highly selective CO2 conversion to formate, Sep. Purif. Technol. 300 (2022), 121848, https://doi.org/10.1016/j.seppur.2022.121848.
[14] L. Fan, C. Xia, P. Zhu, Y. Lu, H. Wang, Electrochemical CO2 reduction to high-concentration pure formic acid solutions in an all-solid-state reactor, Nat. Commun. 11 (2020) 1–9, https://doi.org/10.1038/s41467-020-17403-1.
[15] M. Ramdin, A.R.T. Morrison, M. De Groen, R. Van Haperen, R. De Kler, E. Irtem, A. T. Laitinen, L.J.P. Van Den Broeke, T. Breugelmans, J.P.M. Trusler, W. De Jong, T. J.H. Vlugt, High-Pressure Electrochemical Reduction of CO2 to Formic Acid/Formate: Effect of pH on the Downstream Separation Process and Economics, Ind. Eng. Chem. Res. 58 (2019) 22718–22740, https://doi.org/10.1021/acs.iecr.9b03970.
[16] B.S. Jayathilake, S. Bhattacharya, N. Vaidehi, S.R. Narayanan, Efficient and Selective Electrochemically Driven Enzyme-Catalyzed Reduction of Carbon Dioxide to Formate using Formate Dehydrogenase and an Artificial Cofactor, Acc. Chem. Res. 52 (2019) 676–685, https://doi.org/10.1021/acs.accounts.8b00551.
[17] F. He, A. Hemmatifar, M.Z. Bazant, T.A. Hatton, Selective adsorption of organic anions in a flow cell with asymmetric redox active electrodes, Water Res. 182 (2020), 115963, https://doi.org/10.1016/j.watres.2020.115963.
[18] X. Su, K.J. Tan, J. Elbert, C. Rüttiger, M. Gallei, T.F. Jamison, T.A. Hatton, Asymmetric Faradaic systems for selective electrochemical separations, Energy Environ. Sci. 10 (2017) 1272–1283, https://doi.org/10.1039/c7ee00066a.
[19] X. Su, T.A. Hatton, Redox-electrodes for selective electrochemical separations, Adv. Colloid Interface Sci. 244 (2017) 6–20, https://doi.org/10.1016/j.cis.2016.09.001.
[20] X. Su, H.J. Kulik, T.F. Jamison, T.A. Hatton, Anion-Selective Redox Electrodes: Electrochemically Mediated Separation with Heterogeneous Organometallic Interfaces, Adv. Funct. Mater. 26 (2016) 3394–3404, https://doi.org/10.1002/adfm.201600079.
[21] D.S. Achilleos, T.A. Hatton, Selective Molecularly Mediated Pseudocapacitive Separation of Ionic Species in Solution, ACS Appl. Mater. Interfaces. 8 (2016) 32743–32753, https://doi.org/10.1021/acsami.6b07605.
[22] J.C. Wu, S.S. Chen, T.C. Yu, K.C.W. Wu, C.H. Hou, Effective electrochemically controlled removal of fluoride ions using electrodeposited polyaniline-carbon nanotube composite electrodes, Sep. Purif. Technol. 254 (2021), 117561, https://doi.org/10.1016/j.seppur.2020.117561.
[23] D. Li, L. Huang, Y. Tian, T. Liu, L. Zhen, Y. Feng, Facile synthesis of porous Cu-Sn alloy electrode with prior selectivity of formate in a wide potential range for CO2 electrochemical reduction, Appl. Catal. B Environ. 292 (2021) 1–11, https://doi.org/10.1016/j.apcatb.2021.120119.
[24] B.M. Asquith, J. Meier-Haack, B.P. Ladewig, Poly(arylene ether sulfone) copolymers as binders for capacitive deionization activated carbon electrodes, Chem. Eng. Res. Des. 104 (2015) 81–91, https://doi.org/10.1016/j.cherd.2015.07.020.
[25] W. Xing, J. Liang, W. Tang, D. He, M. Yan, X. Wang, Y. Luo, N. Tang, M. Huang, Versatile applications of capacitive deionization (CDI)-based technologies, Desalination. 482 (2020), https://doi.org/10.1016/j.desal.2020.114390.
[26] S. Bao, B. Chen, Y. Zhang, Y. Cui, Selective adsorption of vanadium in asymmetric capacitive deionization with resin/activated carbon composite electrodes, Chem. Eng. Res. Des. 163 (2020) 107–114, https://doi.org/10.1016/j.cherd.2020.08.015.
[27] R. Uwayid, E.N. Guyes, A.N. Shocron, J. Gilron, M. Elimelech, M.E. Suss, Perfect divalent cation selectivity with capacitive deionization, Water Res. 210 (2022), 117959, https://doi.org/10.1016/j.watres.2021.117959.
[28] A.N. Shocron, R.S. Roth, E.N. Guyes, R. Epsztein, M.E. Suss, Comparison of Ion Selectivity in Electrodialysis and Capacitive Deionization, Environ. Sci. Technol. Lett. 9 (2022) 889–899, https://doi.org/10.1021/acs.estlett.2c00551.
[29] P. Srimuk, X. Su, J. Yoon, D. Aurbach, V. Presser, Charge-transfer materials for electrochemical water desalination, ion separation and the recovery of elements, Nat. Rev. Mater. 5 (2020) 517–538, https://doi.org/10.1038/s41578-020-0193-1.
[30] X. Ma, W. (Alex) Wang, L. Zhang, Q. Wu, S. Lu, D. Aurbach, Y. Xiang,, Anions-capture materials for electrochemical electrode deionization: Mechanism, performance, and development prospects, Desalination. 520 (2021), 115336, https://doi.org/10.1016/j.desal.2021.115336.
[31] F. Chen, J. Wang, C. Feng, J. Ma, T. David Waite, Low energy consumption and mechanism study of redox flow desalination, Chem. Eng. J. 401 (2020), 126111, https://doi.org/10.1016/j.cej.2020.126111.
[32] M.A. Alkhadra, X. Su, M.E. Suss, H. Tian, E.N. Guyes, A.N. Shocron, K.M. Conforti, J.P. De Souza, N. Kim, M. Tedesco, K. Khoiruddin, I.G. Wenten, J.G. Santiago, T. A. Hatton, M.Z. Bazant, Electrochemical Methods for Water Purification, Ion Separations, and Energy Conversion, Chem. Rev. 122 (2022) 13547–13635, https://doi.org/10.1021/acs.chemrev.1c00396.
[33] Z. Hao, X. Sun, J. Chen, X. Zhou, Y. Zhang, Recent Progress and Challenges in Faradic Capacitive Desalination: From Mechanism to Performance, Small. 2300253 (2023) 1–28, https://doi.org/10.1002/smll.202300253.
[34] Q. Li, Y. Zheng, D. Xiao, T. Or, R. Gao, Z. Li, M. Feng, L. Shui, G. Zhou, X. Wang, Z. Chen, Faradaic Electrodes Open a New Era for Capacitive Deionization, Adv. Sci. 7 (2020), https://doi.org/10.1002/advs.202002213.
[35] E.T. Sayed, M. Al Radi, A. Ahmad, M.A. Abdelkareem, H. Alawadhi, M.A. Atieh, A. G. Olabi, Faradic capacitive deionization (FCDI) for desalination and ion removal from wastewater, Chemosphere. 275 (2021). 10.1016/j.chemosphere.2021.130001.
[36] S. Liao, C. Xue, Y. Wang, J. Zheng, X. Hao, G. Guan, A. Abuliti, H. Zhang, G. Ma, Simultaneous separation of iodide and cesium ions from dilute wastewater based on PPy/PTCF and NiHCF/PTCF electrodes using electrochemically switched ion exchange method, Sep. Purif. Technol. 139 (2015) 63–69, https://doi.org/10.1016/j.seppur.2014.11.003.
[37] H. Yoon, J. Lee, S. Kim, J. Yoon, Review of concepts and applications of electrochemical ion separation (EIONS) process, Sep. Purif. Technol. 215 (2019) 190–207, https://doi.org/10.1016/j.seppur.2018.12.071.
[38] A. Suresh, G.T. Hill, E. Hoenig, C. Liu, Electrochemically mediated deionization: A review, Mol. Syst. Des. Eng. 6 (2021) 25–51, https://doi.org/10.1039/d0me00090f.

[39] N. Kim, J. Jeon, R. Chen, X. Su, Electrochemical separation of organic acids and proteins for food and biomanufacturing, Chem. Eng. Res. Des. 178 (2022) 267–288, https://doi.org/10.1016/j.cherd.2021.12.009.
[40] X. Su, A. Kushima, C. Halliday, J. Zhou, J. Li, T.A. Hatton, Electrochemically-mediated selective capture of heavy metal chromium and arsenic oxyanions from water, Nat. Commun. 9 (2018), https://doi.org/10.1038/s41467-018-07159-0.
[41] N. Kim, J. Jeon, J. Elbert, C. Kim, X. Su, Redox-mediated electrochemical desalination for waste valorization in dairy production, Chem. Eng. J. 428 (2022), 131082, https://doi.org/10.1016/j.cej.2021.131082.
[42] X. Su, Electrochemical interfaces for chemical and biomolecular separations, Curr. Opin. Colloid Interface Sci. 46 (2020) 77–93, https://doi.org/10.1016/j.cocis.2020.04.005.
[43] S. Polat, R. Kortlever, H.B. Eral, Ultrasound-promoted preparation of polyvinyl ferrocene-based electrodes for selective formate separation: Experimental design and optimization, Ultrason. Sonochem. 89 (2022), 106146, https://doi.org/10.1016/j.ultsonch.2022.106146.
[44] S. Guo, M.J. Kim, J.C. Siu, N. Von Windheim, K. Gall, S. Lin, B.J. Wiley, Eight-Fold Intensification of Electrochemical Azidooxygenation with a Flow-Through Electrode, ACS Sustain. Chem. Eng. 10 (2022) 7648–7657, https://doi.org/10.1021/acssuschemeng.2c01525.
[45] Y. Qi, X. Chen, D. Huo, H. Liu, M. Yang, C. Hou, Simultaneous detection of Cd2+ and Pb2+ in food based on sensing electrode prepared by conductive carbon paper, rGO and CoZn·MOF (CP-rGO-CoZn·MOF), Anal. Chim. Acta. 1220 (2022), 339812, https://doi.org/10.1016/j.aca.2022.339812.
[46] X. Mao, G.C. Rutledge, T.A. Hatton, Polyvinylferrocene for noncovalent dispersion and redox-controlled precipitation of carbon nanotubes in nonaqueous media, Langmuir. 29 (2013) 9626–9634, https://doi.org/10.1021/la401440w.
[47] X. Mao, F. Simeon, D.S. Achilleos, G.C. Rutledge, T.A. Hatton, Metallocene/carbon hybrids prepared by a solution process for supercapacitor applications, J. Mater. Chem. A. 1 (2013) 13120–13127, https://doi.org/10.1039/c3ta13361c.